10.4 CAN GIANT AEROSOL PARTICLES FAIL TO HELP PRODUCE RAIN?

Colleen K. Henry* and Sonia-Lasher-Trapp
Purdue University, West Lafayette, Indiana

1. INTRODUCTION

While many studies have demonstrated the importance of giant or ultragiant aerosol in expediting warm rain formation (e.g. Szumowski et al. 1999, Johnson 1982, Lasher-Trapp et al. 2001, Blyth et al. 2003), few have focused on identifying large-scale factors that inhibit the giant aerosol from accelerating precipitation formation, such as atmospheric stability and cloud dynamics.

Johnson (1982) investigated the influence of giant aerosol on warm rain formation in maritime and continental clouds using idealized models of droplet growth by condensation and coalescence and showed that giant aerosol can play an important role in precipitation initiation, as well as explain the development of early radar echoes in clouds. His results were limited, however, by a lack of observations with which to constrain the model calculations and to compare the results. Other studies have had similar limitations, such as that by Blyth et al. (2003) who found that coalescence growth onto giant aerosol particles could sufficiently explain the early radar echo observations from the Small Cumulus Microphysics Study, but estimation of the observed giant aerosol was made difficult due to instrument error.

The present study utilizes aircraft and radar data from the Rain in Cumulus over the Ocean (RICO) project, conducted in the winter of 2004-2005 in the Caribbean to compare observations of giant aerosol particles with the behavior of the observed radar echoes. The end goal is to understand under what conditions the giant aerosol ingested into the cloud may not be significant for precipitation initiation. Estimates of the giant aerosol present on each day are produced using data collected in the clear air by the National Center for Atmospheric Research's (NCAR) C-130 aircraft. The NCAR SPol-Ka radar was used to study the evolution of the trade wind cumulus clouds. Because the focus of this project is upon precipitation initiation, flights for analysis were chosen based upon the presence of shallow cumulus clouds, which produced a subset of eleven days for this study.

* *Corresponding author address:* Colleen K. Henry, Purdue University, Earth and Atmospheric Science Department, 550 Stadium Mall Dr., West Lafayette, IN 47907; e-mail: chenry@purdue.edu

2. ANALYSIS METHODS

2.1 *Aircraft Data Analysis*

Wide circles (approximately 9 km in diameter) were flown at the start and end of each flight to evaluate aerosol characteristics and heat and moisture fluxes during RICO. These circles were used to quantify the giant aerosol because they provide long times to observe the aerosol in mostly clear air with limited cloud penetrations. Data from liquid water sensors and particle measuring probes were used for eliminating cloud penetrations from these data (Fig. 1). Lidar data from the aircraft were also scrutinized to check for contamination of the giant aerosol estimates from nearby clouds or precipitation.

Once specific flights and clear air times within the circle patterns were isolated, the particle number concentrations and sizes recorded by the Forward Scattering Spectrometer Probe[1] (FSSP) were averaged versus altitude for each flight. Maximum sizes and concentrations for each period of clear air were plotted versus height and time, as well as averages of these quantities. The averages of maximum concentration and size are time-weighted averages over each height, with no distinction between the circles at the start of each flight and those at the end.

2.2 *Radar Analysis*

The NCAR SPol-Ka radar is a dual-wavelength (10 cm and 8 mm), dual-polarization radar; it scanned the trade wind cumulus clouds predominantly in the Plan-Position Indicator (PPI) mode for RICO. The scanned sectors were oriented along the direction of the mean wind to maximize coverage of all echoes. Volume scans were completed every 3-4 minutes, which allowed ~10 volume scans per typical cloud lifetime.

[1] Manufactured by Particle Measuring Systems, Boulder, CO

The radar data analysis consisted of first identifying reflectivity factor maxima of clouds on each of the eleven days, and recording the corresponding differential reflectivity (ZDR) value at the same spatial and temporal location. The goal is to characterize the size of drops that are forming the maximum reflectivity cores of clouds as they grow and begin to precipitate. In order to obtain consistency between the different days used in this study as well as reproducibility, radar echoes for analysis were limited to a particular sector northeast of Barbuda (0° - 90° azimuth). A maximum radial distance of 45 km from the radar was also imposed because of the resolution decrease with range.

Because the focus of this study is upon precipitation initiation, the analysis was limited to growing clouds, and echoes were followed until they reached their peak reflectivity (when possible). "Maximum reflectivity" as used here is the highest reflectivity seen in a volume scan of an echo, avoiding those created by large frigate birds that were commonly near the radar during RICO, or other non-meteorological targets. Birds and other false echoes were avoided by using the ZDR and radial velocity: because the birds have such a large wingspan, they appear with ZDR values in excess of 4 dB, or below -2.25 dB if oriented vertically, and have anomalous radial velocities relative to neighboring data points.

Once the maximum reflectivity factor for a cloud was identified, the corresponding ZDR value at the same location within the cloud was recorded (Fig. 2). When possible, the same echo was tracked until it reached its "peak maximum reflectivity", the largest reflectivity of all volume scans before the reflectivity begins to decrease in subsequent volume scans. On some days the cloud configuration made tracking of individual clouds from formation to rainfall impossible, so individual points were taken from different echoes. Using this procedure, plots of maximum Z and corresponding ZDR over a field of trade cumulus were generated for all eleven days.

3. PRELIMINARY RESULTS AND DISCUSSION

3.1 *Giant Aerosol Regimes Observed during RICO*

An increase in giant aerosol particle maximum size and concentration with height occurs for most of the RICO flights over the lowest two circles (Figs. 3 and 4). To interpret the increase in maximum size with height (Fig. 3), time-weighted relative humidity for each aerosol sampling altitude was calculated. The relative humidity increased with height by about 10% from the 91m circle to the 458 m circle on most days, before decreasing sharply (as expected) at the 5 km circle. This indicates that most likely the increase in size with height of the detected particles between the bottom two circles can be explained by the onset of deliquescence of the giant salt particles.

The increase in particle concentration with height detected by the FSSP (Fig. 4) can be explained similarly. As the particles rise in the atmosphere from the 91 m circle to the 458 m circle, the hygroscopic sea salt aerosol deliquesce due to increasing relative humidity. At the 91 m level, the smallest giant aerosol particles (≤ 2 μm in diameter) cannot be detected by the FSSP, but as they ascend and begin to deliquesce in response to a higher relative humidity environment, they become detectable by the FSSP, increasing the particle number concentration shown in Figure 3.

The FSSP-detected giant aerosol particle concentrations appear to fall into three regimes (Fig. 4) that correspond to three different regimes in the wind speeds near the ocean surface as measured by the C-130 aircraft dropsondes released during the 5 km circles. The first regime includes the 18 and 19 Jan flights which were characterized by giant aerosol concentrations below 30 L^{-1}, and weak near-surface winds (~ 2 ms^{-1} maximum), the second regime includes all flights in December 2004 as well as 23 Jan 2005 that had stronger near-surface wind speeds of 5-7 ms^{-1}, and the third regime includes the 7, 11, and 14 Jan flights which had the highest concentrations of all the flights and highest near-surface wind speeds (> 11 ms^{-1}). This analysis suggests that the near-surface wind speed governed the giant aerosol concentration regime of each day, consistent with previous studies of sea salt dispersal into the atmosphere (e.g. Woodcock 1953, Blanchard and Syzdek 1972).

3.2 *Radar Echo Evolution Inconsistencies with Expected Aerosol Growth of Drops Originating upon Giant Aerosol*

Knowing the trends in giant aerosol concentration and size from the aircraft data, the radar data can provide insight into the effects of the giant aerosol on precipitation formation. It is expected that giant aerosol would grow into larger droplets more quickly than smaller CCN, and accelerate the onset of precipitation. This should translate into a greater initial radar reflectivity in the clouds, and a more rapid increase in

reflectivity with time than in cases with few or no giant aerosol. In addition, the change in reflectivity can be viewed as a proxy for time, and the change in differential reflectivity versus reflectivity will thus reveal information about the speed of drop growth. Based solely on giant aerosol influences, days characterized by high concentrations of giant aerosol would be expected to produce large cloud drops (large values of differential reflectivity) quickly, and thus help form precipitation (appreciable reflectivity) more quickly. If this relationship does not hold, one would expect that other factors are regulating the importance of the giant aerosol to rain formation.

One example where this relationship between giant aerosol and rain formation does not appear to hold occurred on 11 Jan 2005 (Fig. 5). Despite having a very high concentration of giant aerosol (Fig. 4), radar echoes did not reach appreciable reflectivities (for the most part < 20 dBZ) and ZDR values remained low (mostly < 0.5 dB). This is unexpected because the abundance of giant aerosol should produce large drops and rapid precipitation onset.

Conversely, the giant aerosol on 19 Jan 2005 fell into the "low" giant aerosol concentration regime (Fig. 4), but was unexpectedly characterized by radar echoes with high relatively and ZDR (Fig. 6). The trend in reflectivity with ZDR is suggestive of another factor dominating rain formation on this day, because such high reflectivities would not be expected if giant aerosol were the only influence.

Other cases where the expected giant aerosol-rain formation relationship does not appear to hold include 7 Dec 2004 and 20 Dec 2004. These cases were characterized by the "middle" giant aerosol regime (Fig. 4), yet exhibited very low reflectivity and ZDR (Figs. 7 and 8), suggesting that other factor(s) may have limited their influence.

3.3 Future Work

Because giant aerosol are not the only factor affecting rain formation, an intensive investigation into the environmental conditions (winds, trade inversion height, etc.) on each day will be conducted with attention to their possible effects on giant aerosol influences. Both environmental soundings and aircraft penetrations of the clouds will be used to investigate these aspects.

Once various potential factors are identified, a typical cloud on each day of interest will be simulated using a 3-D dynamical cloud model, along with a continuous collection trajectory model to estimate the growth of the giant aerosol as they are ingested and grow in the simulated cloud, similar to the approach of Lasher-Trapp et al. 2001. Using the RICO observations to constrain these calculations, the growth of the giant aerosol can be compared to the observed radar echo development to understand the limiting factors on giant aerosol growth for these RICO cases where the radar echo development appears inconsistent with the expected giant aerosol influence upon precipitation development in the clouds.

ACKNOWLEDGEMENTS

The authors gratefully acknowledge all the participants of the RICO field project for their work in collecting these data. This study was funded by grant ATM-0342421 from the National Science Foundation.

4. REFERENCES

Blanchard, D. C and L. Syzdek, 1972. Variations in Aitken and giant nuclei and marine air. *J. Phys. Oceanography*, **2**, 255-262.

Blyth, A. M., S. G. Lasher-Trapp, W. A. Cooper, C. A. Knight, and J. Latham, 2003. The role of giant and ultragiant nuclei in the formation of early radar echoes in warm cumulus clouds. *J. Atmos. Sci.*, **60**, 2557-2572.

Johnson, D. B., 1982. The role of giant and ultragiant aerosol particles in warm rain initiation. *J. Atmos. Sci.*, **39**, 448-460.

Lasher-Trapp, S. G., C. A. Knight, J. M. Straka, 2001. Early radar echoes from ultragiant aerosol in a cumulus congestus: Modeling and observations. *J. Atmos. Sci.*, **58**, 3545-3561.

Szumowski, M. J., R. M. Rauber, and H. T. Ochs III, 1999. The microphysical structure and evolution of Hawaiian rainband clouds. Part III: A test of the ultragiant nuclei hypothesis. *J. Atmos. Sci.*, **56**, 1980-2003.

Woodcock, A. H., 1953. Salt nuclei in marine air as a function of altitude and wind force. *J. Meteor.*, **10**, 362-371.

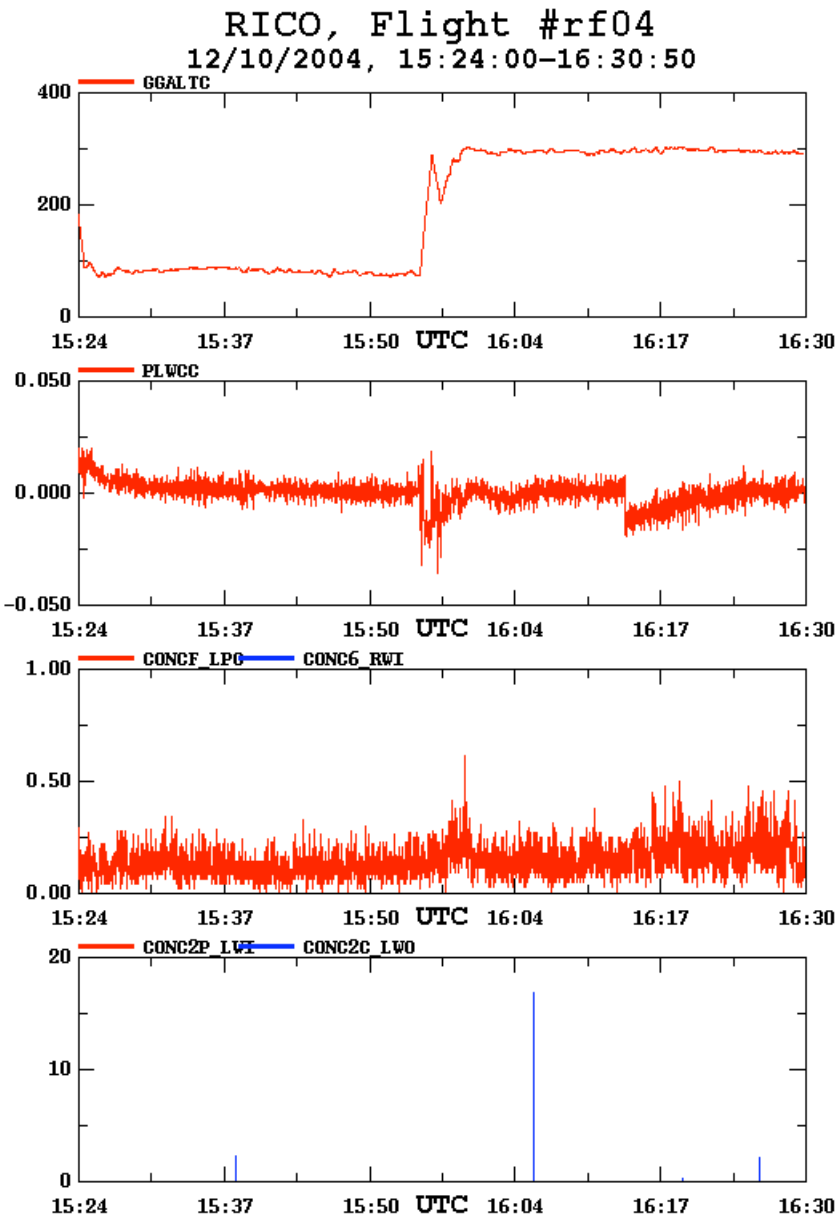

Figure 1. Representative aircraft data from the bottom two circles (90 m and 300 m) flown on 10 Dec 2004. All plots are time series. Top panel shows altitude MSL, middle panel shows liquid water content, third panel shows total particle concentration from FSSP (red line) and 260X (blue line) probes, and the final panel shows particle concentration from 2-DP (red line) and 2-DC (blue line) probes.

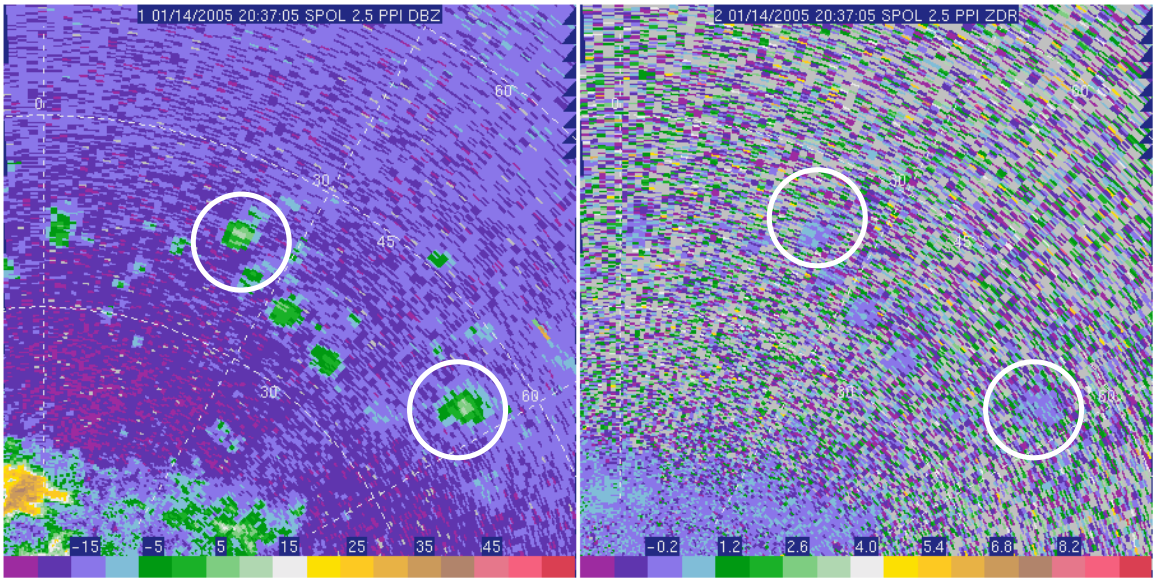

Figure 2. Radar reflectivity factor for two different clouds (circled) on 14 Jan 2005 at 20:37 UTC (left), and corresponding differential reflectivity factor (right).

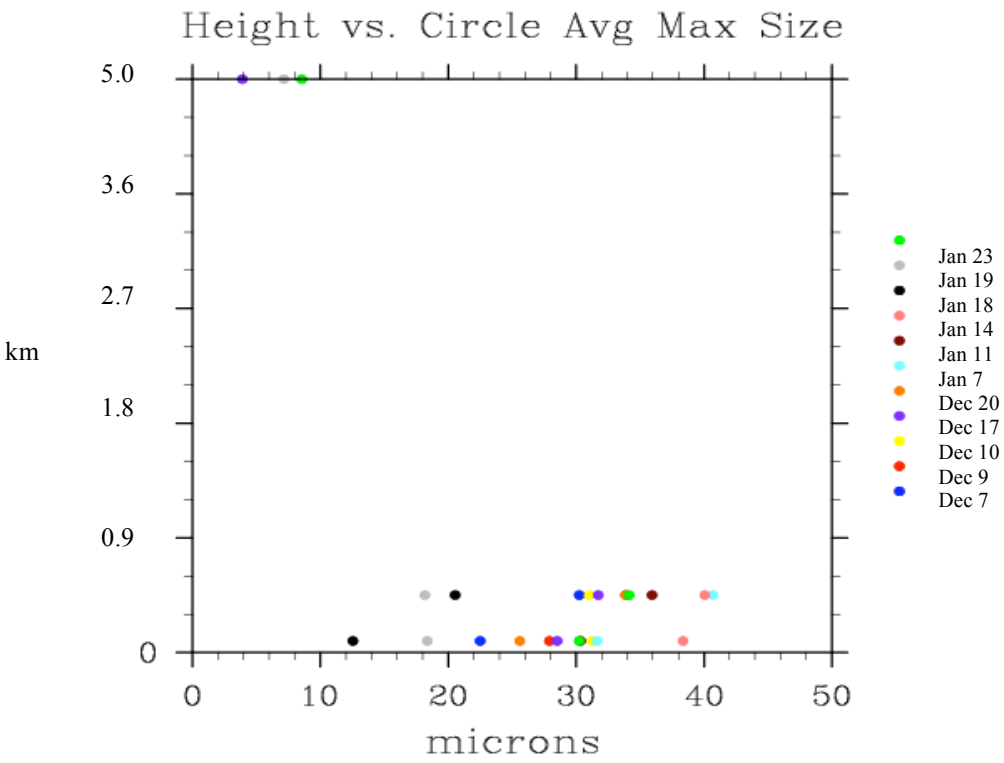

Figure 3. Average maximum particle diameter from FSSP data for all flights investigated for this study. Note the increase with height that is a result of increased deliquescence as the particles move vertically in the atmosphere.

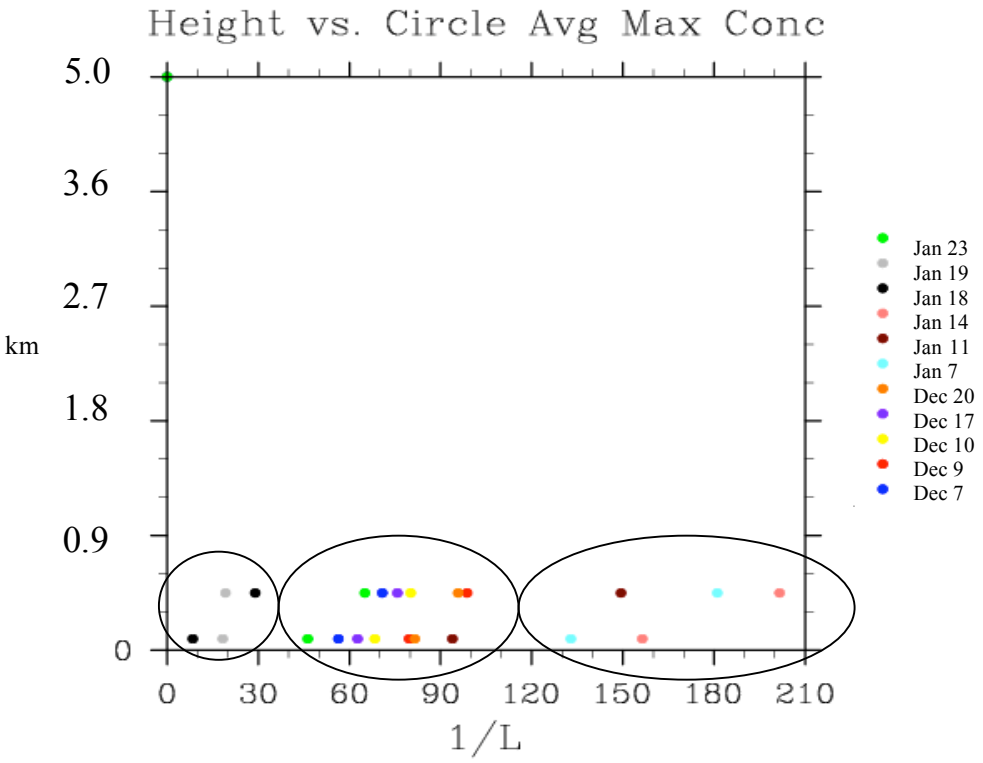

Figure 4. As in Fig. 2, but for maximum concentration. Most concentrations increase with height for the bottom two circles before dropping off severely in the top circle. Three regimes can be seen with small (< $30L^{-1}$), intermediate (30-100 L^{-1}), and high (>100 L^{-1}) concentrations (circled). Those in the "high" regime exhibit a greater increase in particle concentration with height. Uncertainties in these data are less than 1%.

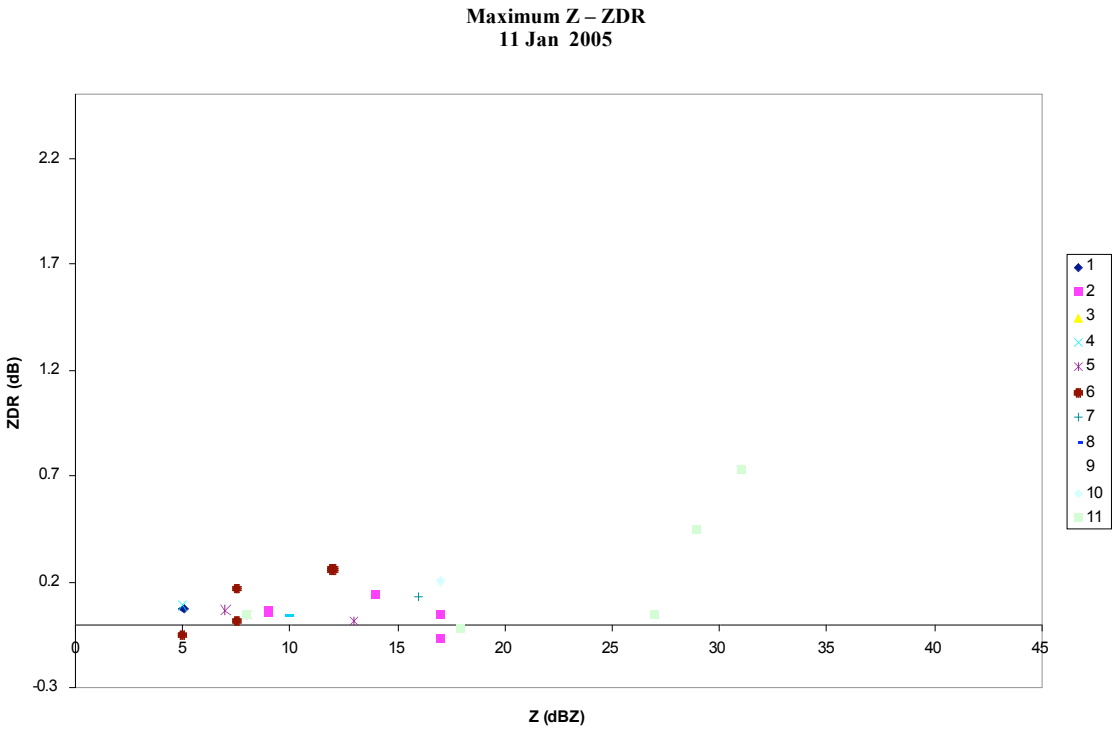

Figure 5. Plot of maximum reflectivity (abscissa) and its corresponding differential reflectivity (ordinate) from 11 Jan 2005. Each symbol represents an individual cloud that was tracked until it reached its peak maximum reflectivity or could no longer be tracked.

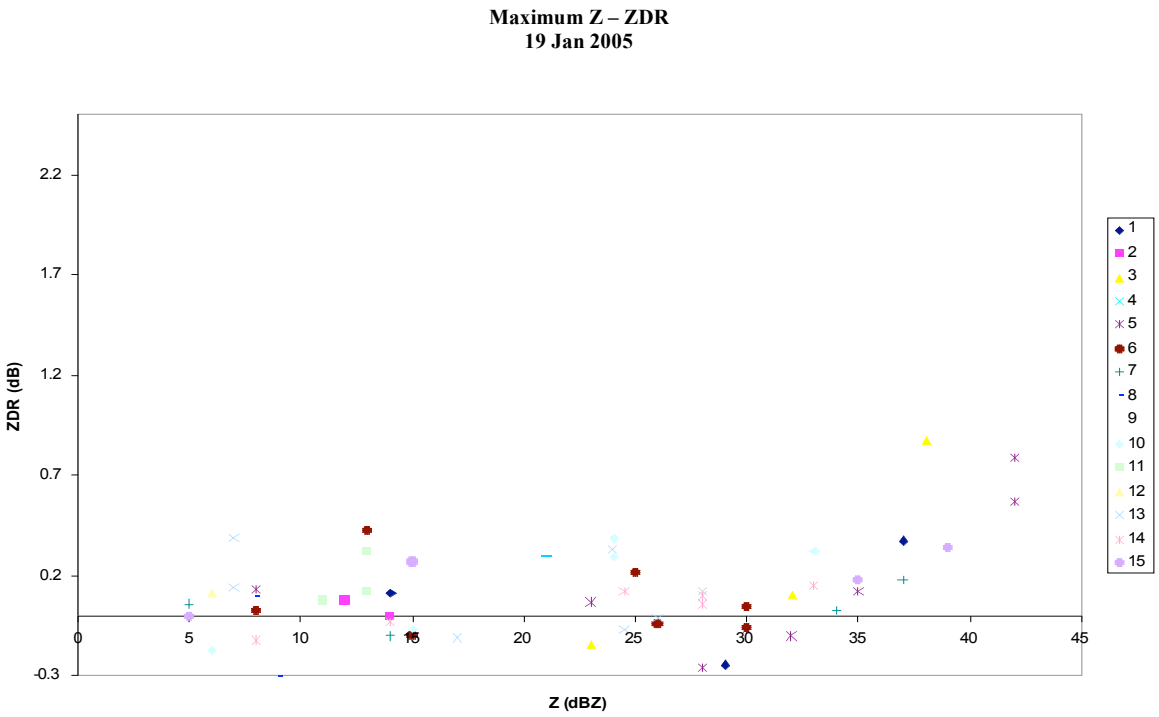

Figure 6. As in Fig. 5, except for 19 Jan 2005.

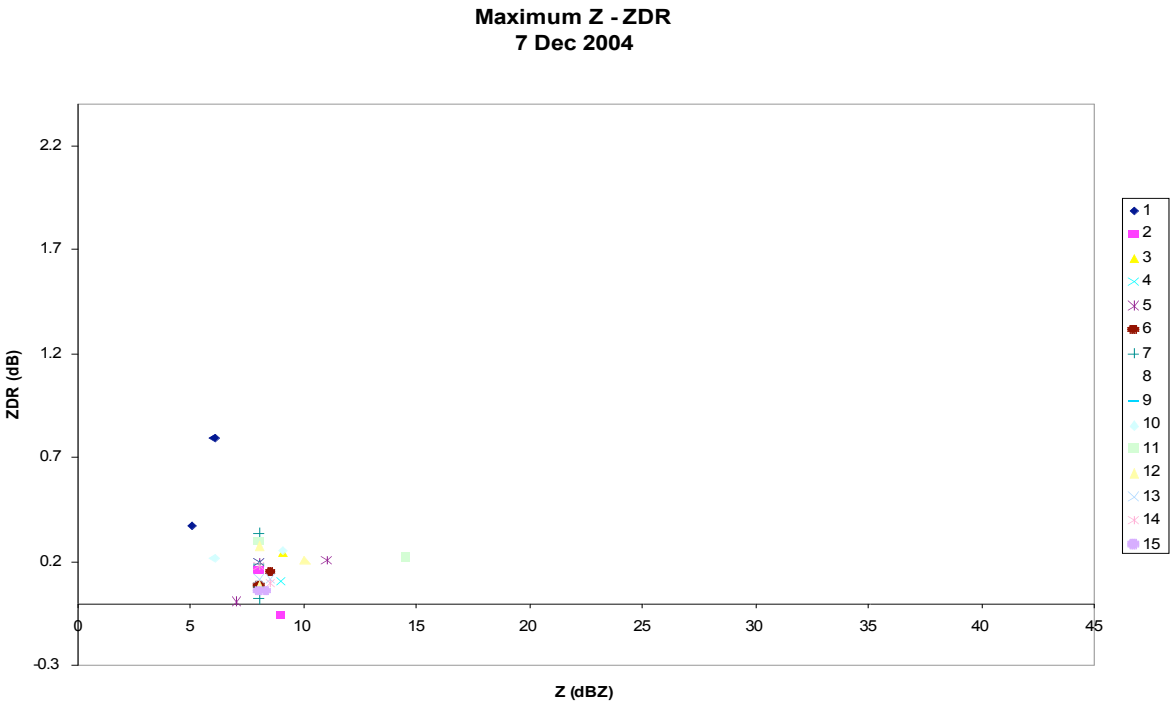

Figure 7. As in Fig. 5, except for 7 Dec 2004.

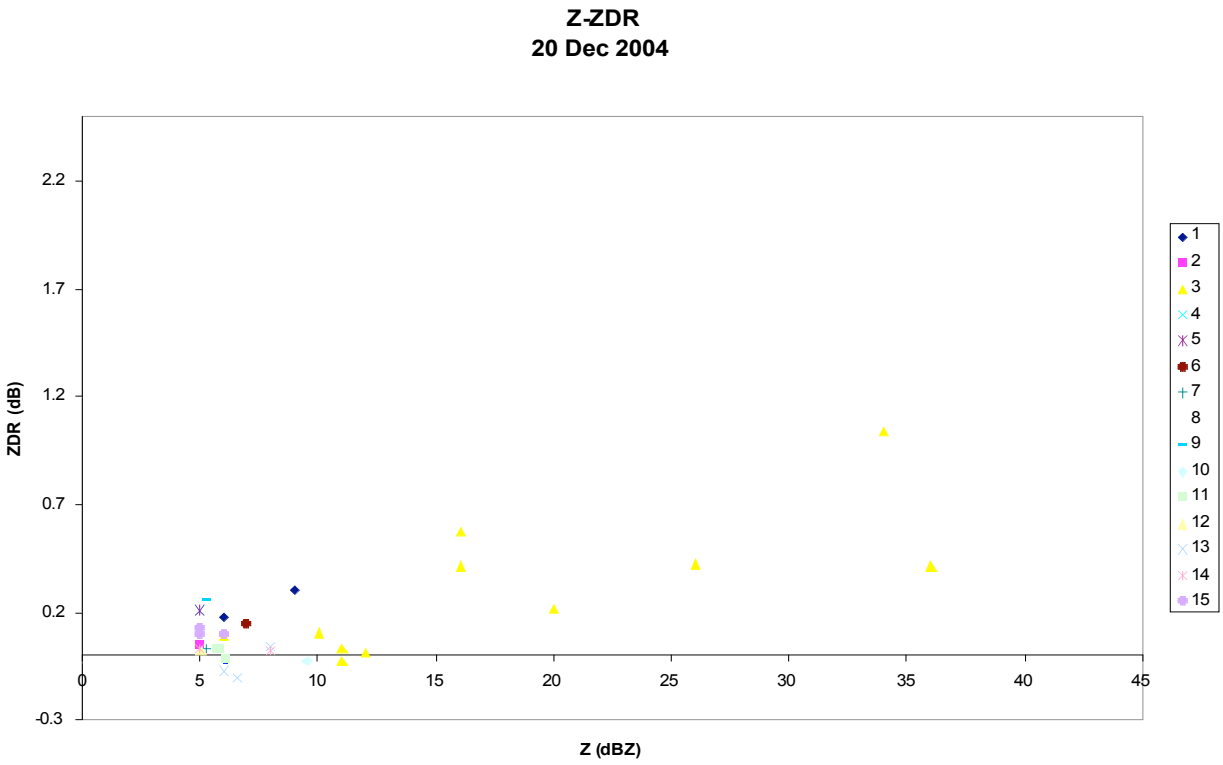

Figure 8. As in Fig. 5, except for 20 Dec 2004.